Supporting Information

Rechargeable Li-ion full batteries based on one-dimensional Li-rich $Li_{1.13}Mn_{0.26}Ni_{0.61}O_2$ cathode and nitrogen-doped carbon-coated NiO anode materials

By *Jong Guk Kim,*[a†] *Yuseong Noh,*[b††] *and Youngmin Kim**[c]

[a]Research Center for Materials Analysis, Korea Basic Science Institute (KBSI), 169-148 Gwahak-ro, Yuseong-gu, Daejeon 34133, Republic of Korea

[b]Department of Chemical Engineering, Pohang University of Science and Technology (POSTECH), 77 Cheongam-Ro, Nam-gu, Pohang, Gyeongbuk 37673, Republic of Korea

[c]Chemical & Process Technology Division, Korea Research Institute of Chemical Technology (KRICT), 141 Gajeong-ro, Yuseong-gu, Daejeon 34114, Republic of Korea

†Present Addresses: Dongwon Systems, 68, Mabang-ro, Seocho-gu, Seoul, Republic of Korea

††Present Addresses: Samsung Electronics, Samsungjeonja-ro, Hwaseong-si, Gyeonggi-do 18448, Republic of Korea

* Corresponding Author: Tel: +82-42-610-8576,

E-mail: ykim@krict.re.kr

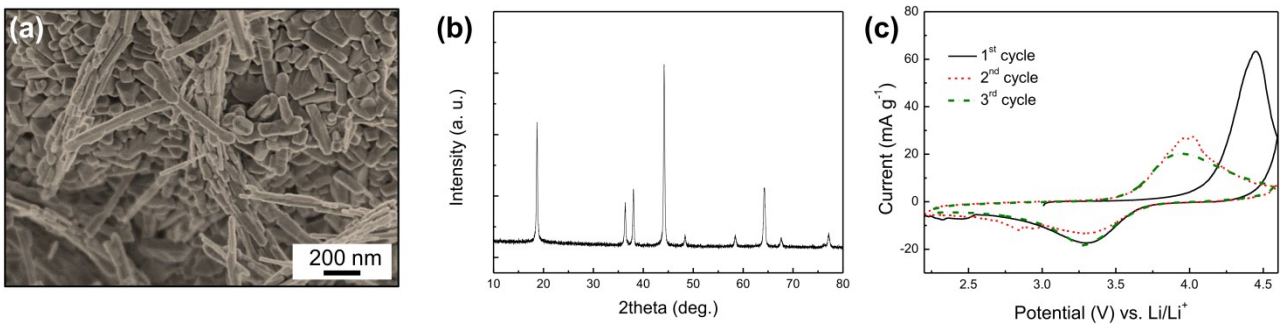

Fig. S1 Typical (a) SEM image and (b) XRD pattern of the pristine LNO. (c) CVs of pristine LNO electrode between 4.6 and 2.2 V at a scan rate of 0.05 mV s^{-1}.

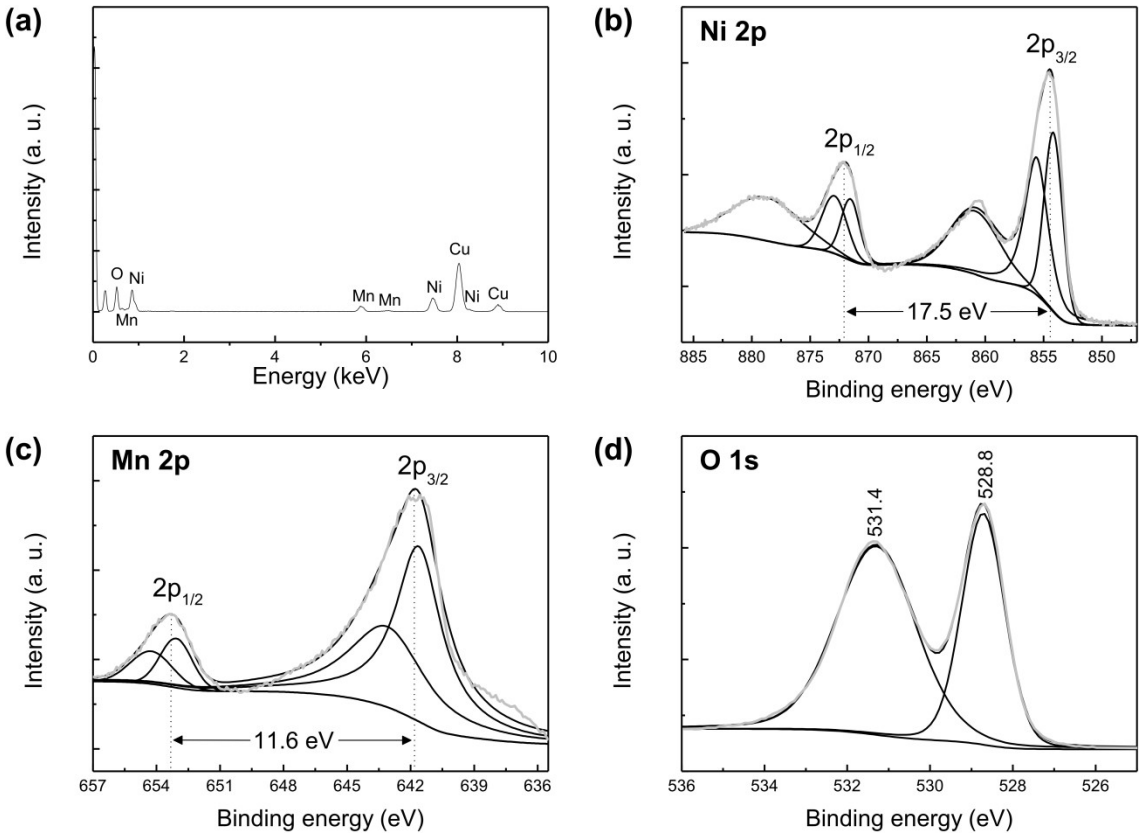

Fig. S2 (a) EDX spectrum of the 1D LMO@LNO. (b-d) XPS spectra of (b) Ni 2p, (c) Mn 2p, and (d) O 1s regions of the 1D LMO@LNO.

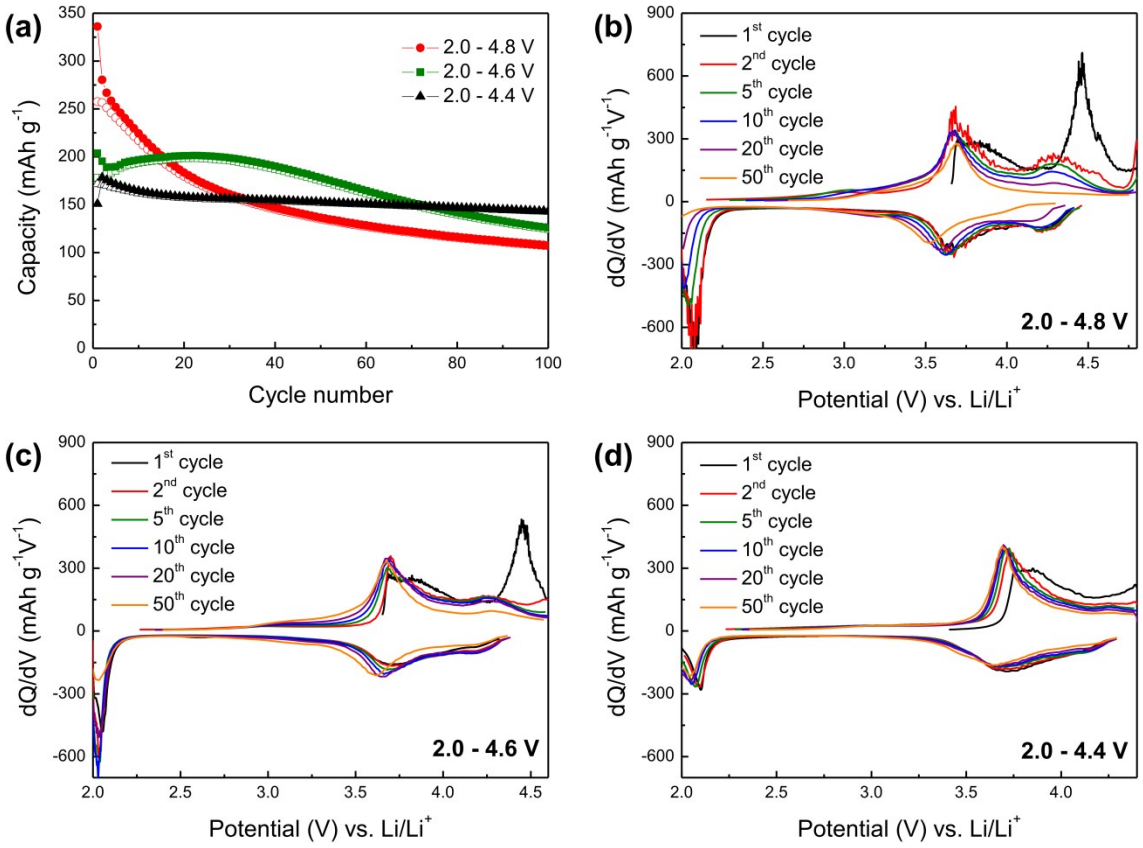

Fig. S3 (a) Cycling performances of the 1D LMO@LNO electrode in the potential window of 2.0-4.8, 2.0-4.6, and 2.0-4.4 V at a current density of 20 mA g^{-1}. (b-d) Corresponding differential capacity plots within the potential window of (b) 2.0-4.8, (c) 2.0-4.6, and (d) 2.0-4.4 V.

Fig. S3 shows the effect of the different charge cutoff voltages on the charge/discharge capacity and capacity retention of the 1D Li-rich LMO@LNO electrode. Obviously, the 1D Li-rich cathode shows better cycling retention at a relatively low charge cutoff voltage because of the suppression of both phase transition and Mn ion migration. Furthermore, because the electrolyte also could be decomposed at a high charge cutoff voltage, lowering the charge cutoff voltage could be a practical way to restrain the capacity of the Li-rich LMO@LNO cathode materials in this study.

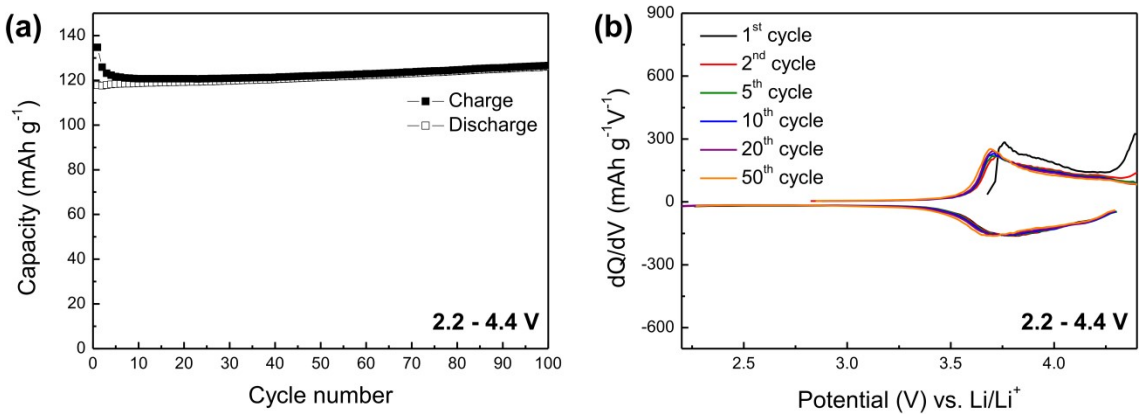

Fig. S4 (a) Cycling performance of the LMO@LNO electrode between 2.2 and 4.4 V at a current density of 20 mA g^{-1}. (b) Corresponding differential capacity plots between 2.2 and 4.4 V.

As shown in Fig. S4, the 1D Li-rich LMO@LNO cathode cycled at a rate of 20 mA g^{-1} in the potential window from 2.2 to 4.4 V for the investigation of the effect of the discharge cutoff voltage on the capacity retention during subsequent cycling. The LMO@LNO displays high stability at a relatively high discharge cutoff voltage, which could originate from the inhibition of the structural deformation.

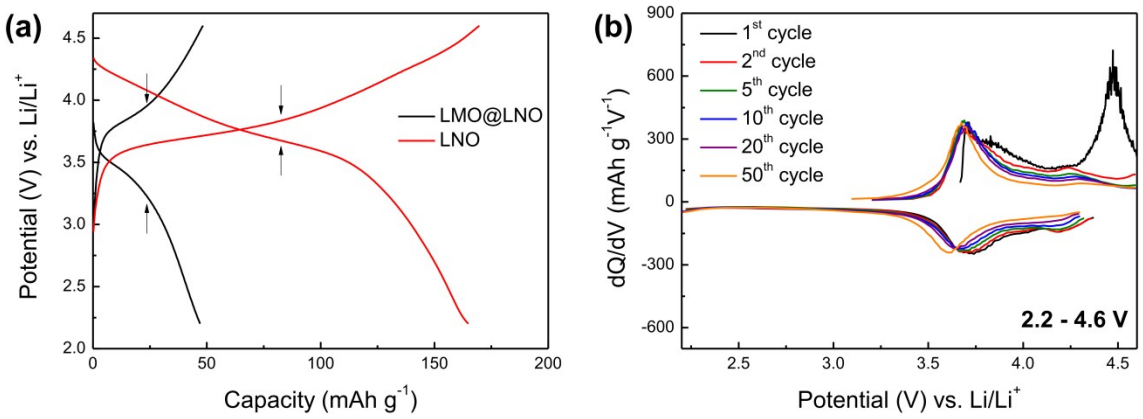

Fig. S5 (a) Charge/discharge capacity-potential curves for the LMO@LNO and pristine LNO electrodes at a current density of 20 mA g^{-1} between 4.6 and 2.2 V at the 11th cycle. The gaps between arrows show the degree of electrode polarization. (b) Differential capacity plots between 2.2 and 4.6 V.

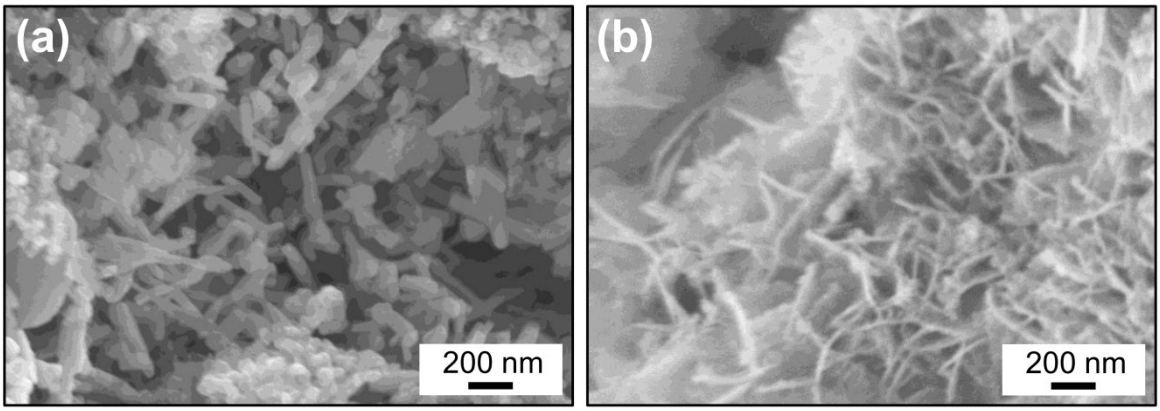

Fig. S6 Typical SEM images of (a) LMO@LNO and (b) NC@NiO electrodes after cyclings in the half-cell.

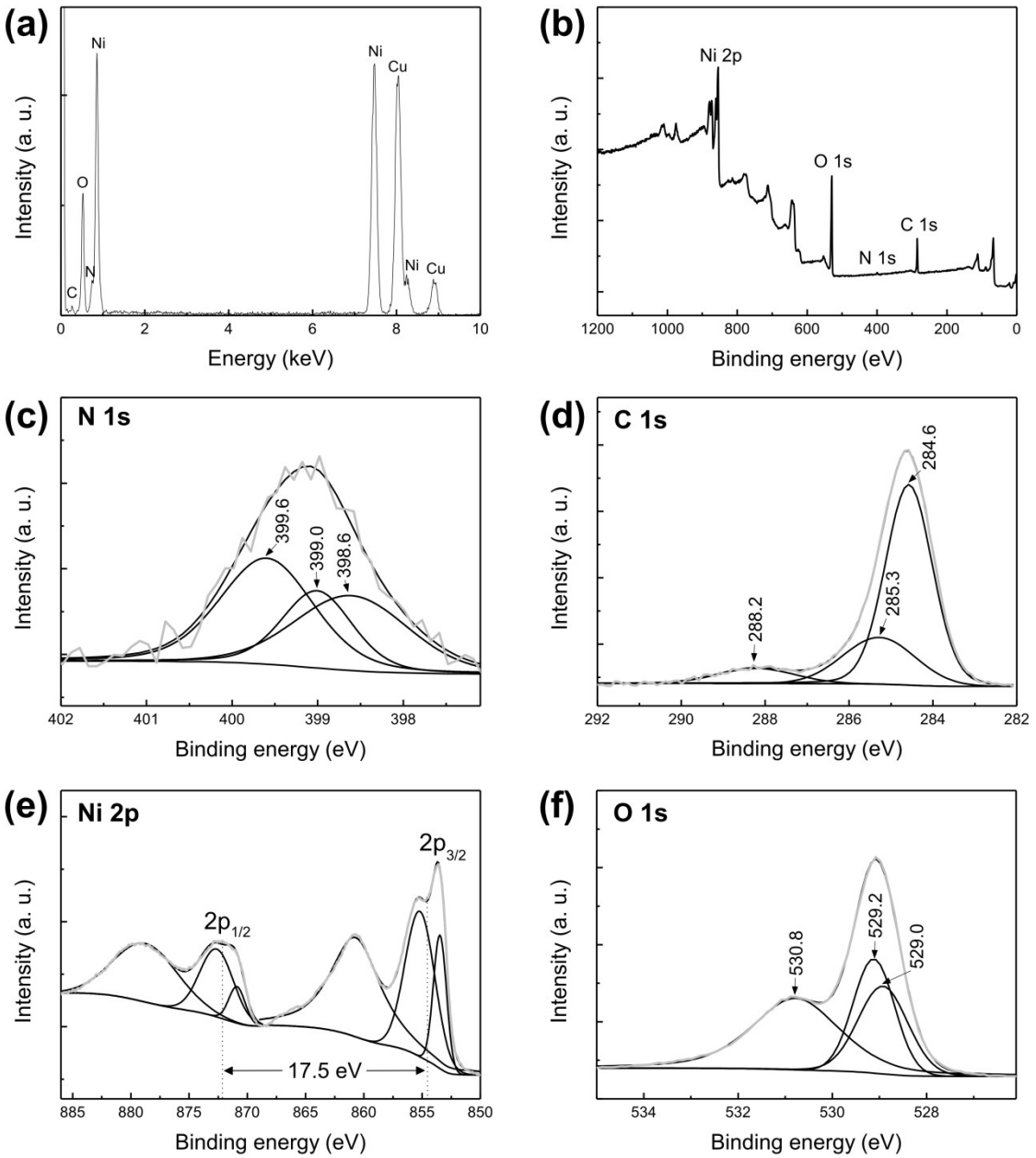

Fig. S7 (a) EDX spectrum of the 1D NC@NiO. (b-f) XPS spectra of (b) full scan, (c) N 1s, (d) C 1s, (e) Ni 2p, and (f) O 1s regions of the 1D NC@NiO.

XPS analysis was performed to examine the oxidation state of the N, C, Ni, and O elements in the as-prepared NC@NiO composite NWs. The XPS survey spectrum of the NC@NiO NWs is depicted in Fig. S7b. As shown in Fig. S7c, the N 1s peak is deconvoluted into three peaks at 399.6, 399.0, and 398.6 eV, which could be attributed to graphitic N, pyrrolic N, and pyridinic N, respectively. Note that the N species could affect the electronic properties of the carbon material through increasing an electron density, resulting in a significant conductivity improvement as compared with non-NC-coated NiO electrode material.[S1] Furthermore, the presence of N heteroatom is able to improve an electrolyte wettability of the electrode.[S2,S3] Fig. S7d presents the C 1s spectrum, which can be resolved into three peak components: the main peak at 284.6 eV is attributed to C–C, whereas minor peaks at 285.3 and 288.2 eV can be assigned to C–O/C-N and C=O/C=N, respectively.[S4] In Fig. S7e, the peaks of 872.2 and 854.7 eV can be attributed to Ni $2p_{1/2}$ and Ni $2p_{3/2}$, respectively. The binding energy separation between these two peaks is 17.5 eV, which is in line with a previous report.[S5] As shown in Fig. S7f, the O 1s peak is deconvoluted into three peaks: one peak at 529.0 eV is ascribed to the oxygen species in the NiO NWs, while the other peaks at 529.2 and 530.8 eV correspond to the OH^- species or chemisorbed oxygen on the surface of NiO NWs.[S6] Consequently, the XPS spectra further demonstrate that the NC@NiO NWs are composed of nitrogen-doped carbon and NiO.

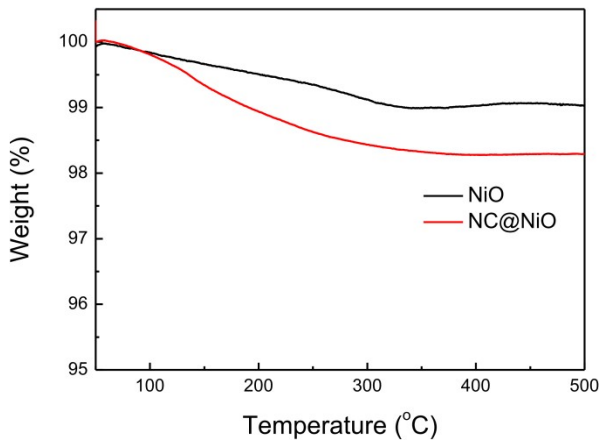

Fig. S8 TGA curves of the non-NC-coated NiO and NC@NiO NWs. The measurements were performed from room temperature to 500 °C at a heating rate of 10 °C min^{-1} in air.

TGA curves were obtained to examine the carbon content in the NC@NiO composites. In Fig. S8, 0.24 % weight loss for both NC@NiO and non-NC-coated NiO NWs before 105 °C was observed, which could be ascribed to the elimination of adsorbed water. 1.01 % weight loss between 105 and 350 °C for the non-NC-coated NiO could originate from the dehydroxylation of surface-attached water and -OH groups, whereas 1.48 % weight loss for the NC@NiO composites could originate from the carbon decomposition. Therefore, the carbon content in the NC@NiO could be 0.47 wt%.

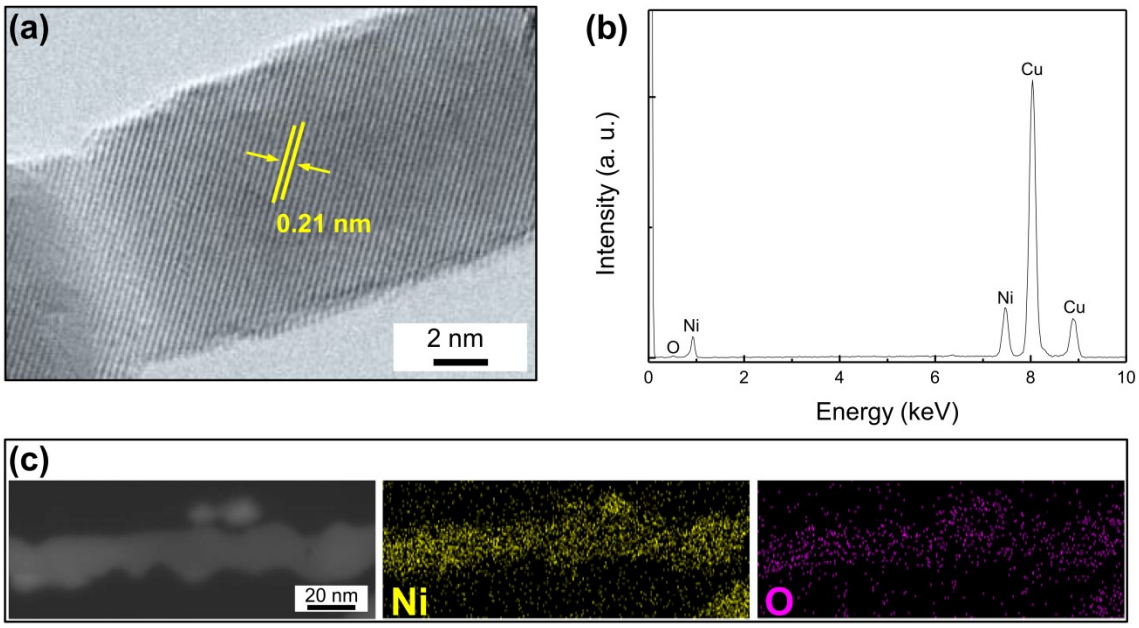

Fig. S9 (a) HRTEM image and (b) EDX spectrum of the non-NC-coated NiO. (c) Darkfield TEM image with corresponding elemental mappings of the Ni and O for the NiO.

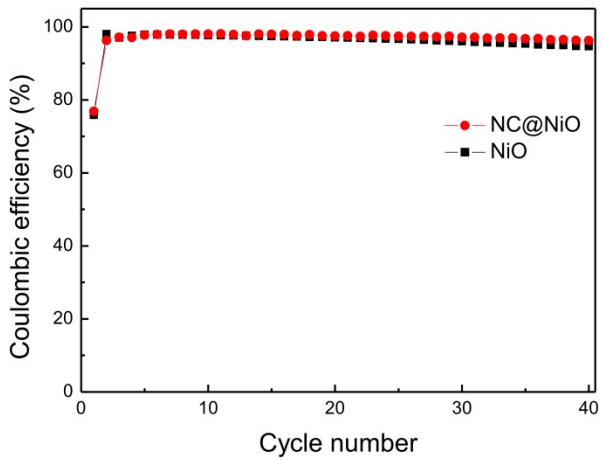

Fig. S10 Coulombic efficiency-cycle number curves of the NC@NiO and NiO at a current rate of 71.8 mA g^{-1} in the potential window of 0.01-3.0 V.

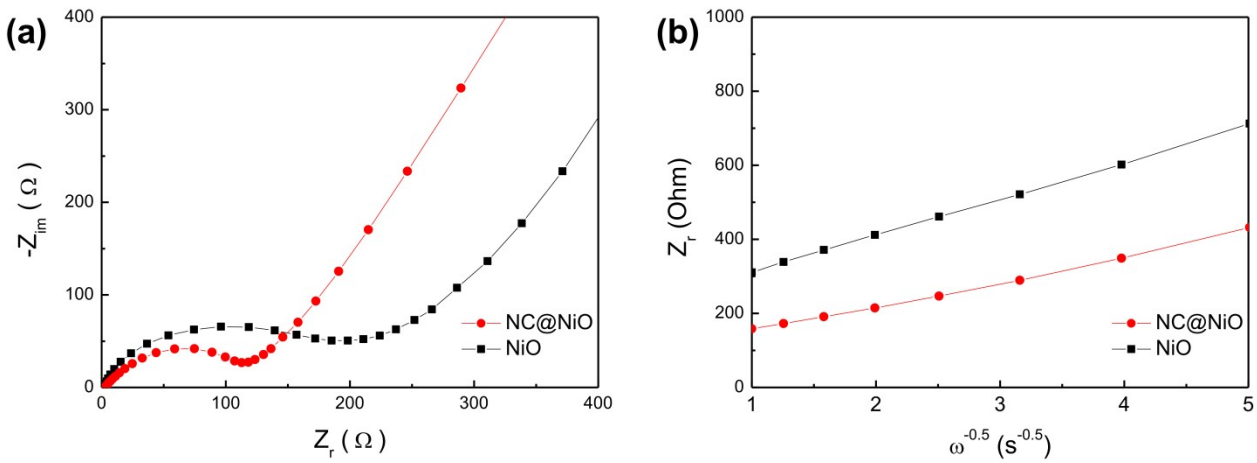

Fig. S11 (a) Nyquist plots of the NC@NiO and NiO measured at 3.0 V after the first. (b) The relationships between Z_r and $\omega^{-0.5}$ after the first cycle.

To examine the kinetic properties of the NC-coated NiO structure, the Li^+ diffusion coefficients (D_{Li+}) of the NC@NiO and NiO electrodes were investigated from EIS measurement (Fig. S11a). The D_{Li+} was obtained by the following equations:

$$D_{Li+} = R^2T^2/2A^2n^4F^4C^2\sigma^2 \quad (1)$$

$$Z_r = R_s + R_{ct} + \sigma\omega^{-0.5} \quad (2)$$

where, R is the gas constant and T is the absolute temperature. A is the electrode area, n is the number of transferred electrons per molecule, F is the Faraday constant, C is the Li^+ concentration, and σ is the Warburg coefficient which is related to Z_r and $\omega^{-0.5}$ from equation (2). By plotting Z_r *vs.* $\omega^{-0.5}$ curves, σ can be explored from the slope in Fig. S11b. According to these parameters, the D_{Li+} of NC@NiO and NiO are 1.94×10^{-18} cm^2 s^{-1} and 7.82×10^{-19} cm^2 s^{-1}, demonstrating the enhanced kinetic properties of the NC@NiO could be originated from its short Li^+ diffusion distance with large electrolyte permeability in the electrode.[S7,S8]

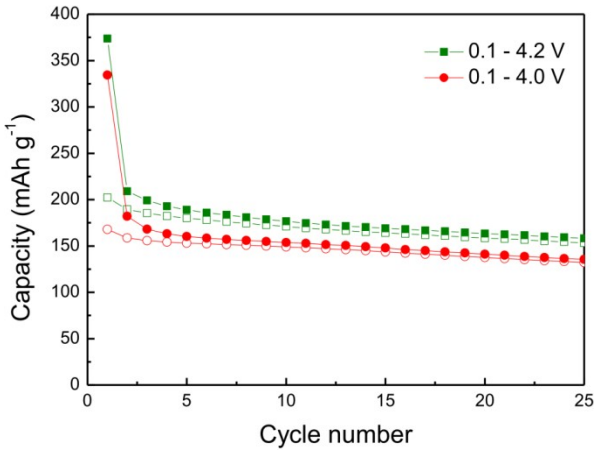

Fig. S12 Cycling performances of the LMO@LNO/NC@NiO (pre-activated) full battery operated at a potential gap of 0.1-4.2 V and 0.1-4.0 V.

The full LIB was also cycled at a current density of 20 mA g^{-1} between 0.1 and 4.2 V to examine the effect of charge cutoff potential on the cycling capacity with cycleability. The full LIB operated from 0.1 to 4.2 V showed higher discharge capacities (153.3 mAh g^{-1}) and lower cycling stability (75.8 %) compared with the discharge capacities (132.1 mAh g^{-1}) and cycleability (78.7 %) of full LIB operated from 0.1 to 4.0 V after 25 cycles.

Table 1 Comparison of performances of the present work with other Li-rich cathode oxides.

Samples	Architecture	Current rate	Cycle number	Capacity retention	Ref.
$0.3Li_2MnO_3 \cdot 0.7LiMn_{0.60}Ni_{0.25}Co_{0.15}O_2$	sphere	0.5 C	30	~175 mAh g^{-1}	S9
$0.3Li_2MnO_3 \cdot 0.7LiMn_{0.60}Ni_{0.25}Co_{0.15}O_2$	particle	0.5 C	25	~170 mAh g^{-1}	S10
$0.3Li_2MnO_3 \cdot 0.7LiMn_{0.7}Ni_{0.2}Co_{0.1}O_2$	particle	0.1 C	30	188 mAh g^{-1}	S11
$0.3Li_2MnO_3 \cdot 0.7LiMn_{1.5}Ni_{0.5}O_4$	particle	50 mA g^{-1}	50	~150 mAh g^{-1}	S12
$0.3Li_2MnO_3 \cdot 0.7LiNi_{0.5}Mn_{0.5}O_2$	particle	5 mA g^{-1}	25	~180 mAh g^{-1}	S13
$0.3Li_2MnO_3 \cdot 0.7LiNi_{0.5}Mn_{0.5}O_2$	sphere	100 mA g^{-1}	80	~150 mAh g^{-1}	S14
$LiCoO_2@Li_2MnO_3$	nanoribbon	10 mA g^{-1}	30	180 mAh g^{-1}	S15
$0.2Li_2MnO_3 \cdot 0.8LiNi_{0.5}Mn_{0.5}O_2$	nanorod	50 mA g^{-1}	100	248 mAh g^{-1}	S16
$0.3Li_2MnO_3 \cdot 0.7LiNi_{1/3}Co_{1/3}Mn_{1/3}O_2$	nanorod	100 mA g^{-1}	60	156 mAh g^{-1}	S17
$0.3Li_2MnO_3 \cdot 0.7LiNiO_2$	nanowire	20 mA g^{-1}	100	139.2 mAh g^{-1}	This work

Table 2 Comparison of charge/discharge properties of the present work with other carbon-coated NiO anode materials.

Samples	Architecture	Current rate	Cycle number	Capacity retention	Ref.
NiO/C	nanocapsule	359 mA g^{-1}	50	1157.7 mAh g^{-1}	S18
NiO/CNTs	microsphere	723 mA g^{-1}	100	549.3 mAh g^{-1}	S19
NiO/C	particle	100 mA g^{-1}	100	625.3mAh g^{-1}	S20
NiO/C	particle	70 mA g^{-1}	50	585.9 mAh g^{-1}	S21
NiO@C	particle	143.6 mA g^{-1}	50	580 mAh g^{-1}	S22
NiO/carbon	nanoweb	100 mA g^{-1}	60	758 mA h g^{-1}	S23
CNS/NiO	nanofiber	100 mA g^{-1}	50	902 mA h g^{-1}	S24
CF/NiO	nanofiber	100 mA g^{-1}	100	441.2 mAh g^{-1}	S25
NiO/C@CNT	microsphere	50 mA g^{-1}	20	573 mAh g^{-1}	S26
NC@NiO	nanowire	71.8 mA g^{-1}	40	1007.2 mAh g^{-1}	This work

References

(S1) M. Gao, L. Yang, B. Dai, X. Guo, Z. Liu and B. Peng, *J. Solid State Electrochem.*, 2016, **20**, 2737-2747.

(S2) X. Xu, F. Niu, C. Wang, Y. Li, C. Zhao, J. Yang and Y. Qian, *Chem. Eng. J.*, 2019, **370**, 606-613.

(S3) D. Cheng, M. Tian, B. Wang, J. Zhang, J. Chen, X. Feng, Z. He, L. Dai and L. Wang, *J. Colloid Interface Sci.*, 2020, **572**, 216-226.

(S4) Y. Ni, Y. Yin, P. Wu, H. Zhang and C. Cai, *ACS Appl. Mater. Interfaces*, 2014, **6**, 7346-7355.

(S5) W. Huang, S. Ding, Y. Chen, W. Hao, X. Lai, J. Peng, J. Tu, Y. Cao and X. Li, *Sci. Rep.*, 2017, **7**, 5220.

(S6) M. Guo, J. Balamurugan, X. Li, N. H. Kim and J. H. Lee, *Small*, 2017, **13**, 1701275.

(S7) F. Wu, J. Dong, L. Chen, L. Bao, N. Li, D. Cao, Y. Lu, R. Xue, N. Liu, L. Wei, Z. Wang, S. Chen and Y. Su, *Energy Storage Mater.*, 2021, **41**, 495-504.

(S8) Y. Wang, Z.-Y. He, Y.-X. Wang, C. Fan, C.-R.-L. Liu, Q.-L. Peng, J.-J. Chen and Z.-S. Feng, *J. Colloid Interface Sci.*, 2018, **512**, 398-403.

(S9) S.-M. Kim, B.-S. Jin, S.-M. Lee and H.-S. Kim, *Electrochim.* Acta, 2015, **171**, 35-41.

(S10) M. Choi, G. Ham, B.-S. Jin, S.-M. Lee, Y. M. Lee, G. Wang and H.-S. Kim, *J. Alloys Compd.*, 2014, **608**, 110-117.

(S11) J.-H. Jeong, B.-S. Jin, W.-S. Kim, G. Wang and H.-S. Kim, *J. Power Sources*, 2011, **196**, 3439-3442.

(S12) P. P. Dahiya, J. Patra, J.-K. Chang, K. Sahoo, S. B. Majumder and S. Basu, *J. Taiwan Inst. Chem. Eng.*, 2019, **95**, 195-201.

(S13) J. Shojan, C. V. Rao, L. Torres, G. Singh and R. S. Katiyar, *Mater. Lett.*, 2013, **104**, 57-60.

(S14) E. Zhao, Z. Hu, L. Xie, X. Chen, X. Xiao and X. Liu, *RSC Adv.*, 2015, **5**, 31238-31244.

(S15) F. X. Wang, S. Y. Xiao, Z. Chang, M. X. Li, Y. P. Wu and R. Holze, *Int. J. Electrochem. Sci.*, 2014, **9**, 6182-6190.

(S16) J. Yang, F. Cheng, X. Zhang, H. Gao, Z. Tao and J. Chen, *J. Mater. Chem. A*, 2014, **2**, 1636-1640.

(S17) C. Zhao, Z. Hu and Q. Shen, *Micro Nano Lett.*, 2015, **10**, 122-125.

(S18) X. Liu, S. W. Or, C. Jin, Y. Lv, C. Feng and Y. Sun, *Carbon*, 2013, **60**, 215-220.

(S19) W. Cao, A. Hu, X. Chen, X. Liu, P. Liu, Q. Tang and X. S. Zhao, *Electrochim. Acta*, 2016, **213**, 75-82.

(S20) G. Li, Y. Li, J. Chen, P. Zhao, D. Li, Y. Dong and L. Zhang, *Electrochim. Acta*, 2017, **245**, 941-948.

(S21) L. Zhang, J. Mu, Z. Wang, G. Li, Y. Zhang and Y. He, *J. Alloys Compd.*, 2016, **671**, 60-65.

(S22) S. Wei, D. D. Lecce, R. Brescia, G. Pugliese, P. R. Shearing and J. Hassoun, *J. Alloys Compd.*, 2020, **844**, 155365.

(S23) Y. Ma, L. Sheng, H. Zhao, K. An, L. Yu, J. Xu and X. Zhao, *Solid State Sci.*, 2015, **46**, 49-55.

(S24) B. S. Lalia, A. Khalil, T. Shah and R. Hashaikeh, *Ionics*, 2015, **21**, 2755-2762.

(S25) Q. Han, M. Shi, Z. Han, W. Zhang, Y. Li, X. Zhang and Y. Sheng, *Ionics*, 2020, **26**, 5935-5940.

(S26) Z. Jiapan, M. Hongyu, W. Jide, C. Qingxia and Z. Jialiang, *Rare Metal Mat. Eng.*, 2015, **44**, 2109-2113.